Journal of Manufacturing Processes 37 (2019) 339–347

Contents lists available at ScienceDirect

Journal of Manufacturing Processes

journal homepage: www.elsevier.com/locate/manpro

FDM 3D printing of MWCNT re-inforced ABS nano-composite parts with enhanced mechanical and electrical properties

H. Kürşad Sezer*, Oğulcan Eren

Gazi University, Department of Industrial Design Engineering, Teknikokullar, Ankara, Turkey

ARTICLE INFO

Keywords:
Additive manufacturing
3D printing
Mechanical properties
Electrical properties

ABSTRACT

This work presents significant mechanical and electrical property enhancement of 3D printed parts through dispersion of multiwall carbon nanotubes (MWCNTs) using twin-screw micro-compounding extruder having a backflow channel facility. The composite structure obtained has been further processed in a single screw extruder to produce 3D printing filaments, 1,7 mm in diameter. The mechanical, electrical and melt flow properties of the MWCNT reinforced ABS matrix composite parts, with loading percentages up to 10% has been presented for the first time in this work, using a commercial 3D printer. Moreover effects of raster angle on tensile properties such as tensile strength, ductility and the elastic modulus as well as the electrical conductivity are also studied. The tensile strength of 3D printed parts has increased considerably (up to 58 MPa equaivalent to 288% increase) with 7 wt.% addition of MWCNTs in ABS. However ductile to brittle transition was observed with increasing MWCNT concentraion. Micro Raman spectroscopic and scanning electron microscopic analysis made on the 3D-printed MWCNT parts supports the enhanced mechanical properties. Electrical conductivity of the composites has also shown dramatic increase (~ 7 fold increase), owing to the existance of MWCNT particles. A 3 wt.% MWCNT loading percolation threshold found for the linear printing direction shifted to 5 wt.% for the crossed layered samples.

1. Introduction

Additive manufacturing (AM) is a cluster of developing technologies that produce parts layer by layer, one cross-section at a time [1]. Recently, the technology is widely recognised with more famous 3D printing (3DP) term which can be described as the rapid manufacture of 3D parts direct from computer aided design (CAD) data. In fact, both AM and the 3D printing processes fabricate 3D objects with layers added on top of each other directly from CAD data without the need for molds [2]. The process begins by exporting the 3D CAD model of the part to the AM software that controls the machine, in STL format. The STL model is then sliced into smallest possible layers and the slice information are sent to the 3D printer to generate the corresponding layers. The slices are printed one after the other until the part is completed. Printing of each layer may vary depending on the 3D printer used [3]. Metal, polymer or ceramic materials spread in powder form on a tray is sintered / melted by laser or electron beam (Selective Laser Sintering/Melting – SLS/SLM) or using a suitable liquid binder (3D Printing) can be solidified to desired pattern [4,5]. Some machines cure photopolymer resins with UV or visible light performing 3D lithographic processes (Stereolithography Apparatus) [6], others directly deposit fused plastic filaments known as Fused Deposition Modelling (FDM) technology [7,8]. The working principle of the latter is simple as extrusion of a molten thermoplastic filament from a heated nozzle on to a platform. The molten filament flowing through the nozzle orifice impinges on the pre-deposit layers, adheres onto it and quickly solidifies to form the 3D part.

Various advantages of the AM technologies include freedom of design constraints, reduced waste and minimized health & safety hazards excluding the harmful chemicals for etching and cleaning solutions as compared to traditionally used technologies [9]. Fabricating complex organic surfaces and geometries are possible with AM [10]. Moreover, functional moving parts can be created as assembled with tight tolerances. Despite these design and environmental advantages, FDM 3D printing has not effectively been adopted for fabricating the end-use components due to the limited number of existing materials. Currently proprietary polymer materials, such as ABS (Acrylonitrile butadiene styrene), PC (Polycarbonate), PLA (polylactic acid), PA (polyamide) or a combination of them, are mostly used by the modern FDM techniques [11]. However, the mechanical strength is usually lower as compared to conventionally produced parts [12–14]. Besides, mechanical properties usually exhibit different values when measured in different directions

* Corresponding author.
E-mail address: kursadsezer@gazi.edu.tr (H.K. Sezer).

https://doi.org/10.1016/j.jmapro.2018.12.004
Received 20 December 2017; Received in revised form 27 July 2018; Accepted 2 December 2018
Available online 12 December 2018

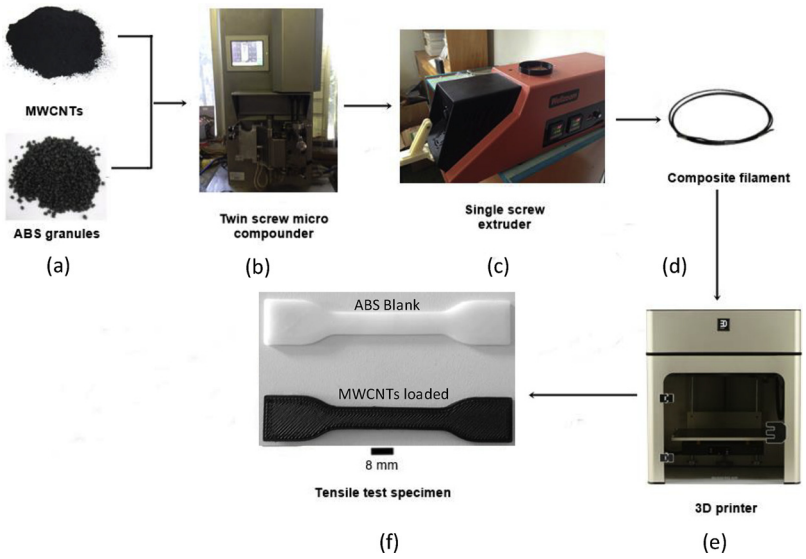

Fig. 1. Nano-Composite filament preparation and 3D printing. a) Picture of MWCNTs particle and ABS ganules b) Dispersions of MWCNTs and ABS with double-screw extruder. c) Making a MWCNTs / ABS composite composite material into a standard filament that can be used with a single-screw extruder in a commercial 3D printing machine. d) MWCNT/ABS nanocomposite Filament winding in rolls. e) Schematic representation of Fused Deposition Modelling (FDM) 3D printing process. The filament is laid in a molten state by means of a heated nozzle on building table which was set at a temperature of 110 °C. f) A typical 3D printed tensile test sample using 5% by weight MWCNTs-ABS composite filament.

owing to the layer by layer manufacturing approach [15]. Although not well-established method, FDM 3D printing of composites by addition of carbon fiber or carbon nanotube (CNT) fillers in one of these proprietary polymers can well-increase the strength of 3D parts [15,16]. Especially addition of the carbon nanotubes (CNTs) fillers can potentially improve properties such as electrical/heat conduction, mechanical strength, modulus of elasticity, toughness, and durability of 3D printed nano-composites for many potential applications [17–20]. Nano-particle filled polymer matrix composites potentially revolutionize many industrial applications in aerospace, defence, automotive, textile and energy fields with their unique mechanical and electrical properties [21]. CNTs has been used as reinforcing agents for high performance polymer composites [22–28]. One of the very first nano-composites with CNT filler particles was introduced by Ajayan et al. in early 90's [29]. Matrices used to firmly hold the nano-particles together can be of thermoplastic [30–37] thermoset type resins [38] or liquid crystalline polymers [19] and others like a biomaterial [32] as reported by a number of researchers. Unique properties, both mechanical and electrical, can be obtained with CNT reinforcements including toughness, tensile strength and modulus, thermal and electrical conductivity etc. [39–44]. As the filler material in the insulating matrix increases, above a percolation threshold, it is possible to observe a conductive path in the polymer matrix created by clusters of filler particles [18]. The desired functional properties are obtained by altering the matrix, reinforcing and processing processes.

Many other research and development studies with successful production of nano-composites containing CNTs are available in open literature. Kennedy et al. have used PVDF-MWCNT composites as a new filament material for FDM derived objects with chemiresistive properties in response to volatile organic compounds [10]. Leigh et al. present formulation of a simple conductive thermoplastic composite which called as a 'carbomorph' and used in a commercial 3D printer to print electronic sensors able to sense mechanical flexing and capacitance changes [17]. Gnanasekarana et al. have studied the process of constructing functional 3D model structures using PPT as polymer, CNT and graphene as reinforcements. They observed the printability, electrical conductivity and mechanical properties of polymer nano-composites before and after 3D printing [19]. Kwok et al. studied on preparation and characterization of PP/Carbon Black thermoplastic composites suitable for electrical circuit printing using FDM-based 3D printing. They also conduct various stress test such as UV [34]. Kumar et al. have developed a new CNC assisted FDM process for the manufacture of flexible electrically conductive Ethylene vinyl acetate/ graphite polymer composite objects [35]. Christ et al. were created TPU/MWCNT nano-composites with various MWCNT content up to 5 wt.%. They noted that besides increasing mechanical, electrical, and piezo-resistive behaviors, MWNCT greatly enhanced the printing capability of soft TPU by increasing the resistance to buckling [36]. Wei et al. reported that the nano-composite they obtained by synthesizing graphene and ABS solutions had superior thermal and electrical conductivity [37]. Mu et al. have been used MWCNTs dispersed in a photocurable resin to obtained electrically conductive objects with DLP (digital light processing) based 3D printing process [38]. Dorigato et al. have been produced nano-composite samples both compression molded (CM) and filament extrusion method then compared their mechanical and electrical properties [44].

MWCNTs filled ABS nano-composite research reported here will include work on establishing procedures for making ABS matrix MWCNTs filler nano-composites for up to 10 wt.% loading in filament form suitable for commercial FDM 3D printing and 3D printing tests with linear and crossed layering approaches for potential improvements of mechanical and electrical properties.

2. Experimental procedures

2.1. Materials

ABS and the MWCNTs were purchased from different commercial suppliers. ABS (Specific gravity 1.05 g/cm^3) was provided in granulated form. Thin MWCNTs (with 9.5 nm average diameter, 1.5 μm average length and 250-300 m^2/g surface area) are produced with 90% carbon purity via the catalytic carbon vapor deposition (CCVD) process. The full procedure of combining the MWCNTs with the ABS to make the composite material are given below.

2.2. Fabrication of MWCNTs/ABS filaments

Schematic diagram of the nano-composite filament preparation and 3D printing process of the MWCNTs/ABS composite filament is shown in Fig. 1. A twin screw micro extruder (DSM Xplore) was used to compound the ABS with MWCNTs. Throughout the MWCNTs dispersion process in ABS matrix the screw speed was kept at 100 rpm. Complete melting and mixing was ensured by maintaining the extruder temperature at 240 °C to avoid degradation of the ABS. Total mixing time was 5 min. Melt was permitted to run into the backflow channel of the extruder for better dispersion during the process. The MWCNT/ABS nano-composite composite samples were prepared with 4 different loadings (i.e. weight % of 1, 3, 5, 7 and 10).

Table 1
3D printing parameters used for the MWCNT filled ABS composite tensile test specimens.

Nozzle diameter - mm	0,4
Layer thickness – mm	0,2
Infill rate (%)	100
Platform temperature – °C	110
Extrusion temperature – °C	245
Printing speed – mm/min	1800

The obtained MWCNTs reinforced ABS composite has been further processed in a single screw extruder (Wellzoom C) to produce filaments (1.7 mm in diameter) suitable for the FDM 3D printer. The granulated composite is preheated to 220 °C and extredud at 2000–2200 mm/min rate to filament form at 235 °C. The obtained MWCNTs filled composite filaments were then used for printing 3D objects.

2.3. 3D printing of composite parts

The commercial FDM 3D printer used was 3Dison Pro from 3disonprinter.com. Tensile test specimens based on ASTM D412 A standard (scaled by 70%) were printed using the composite filaments with 1, 3, 5, 7 and 10 wt percentages of MWCNT loadings. A blank ABS (0% MWCNTs) sample was also prepared. 3 specimens were printed for all different loading percentages. 3D printing parameters used for the test specimens are shown in Table 1. As the objective of the study is to establish mechanical and electrical resistance responses of the MWCNTs loading into ABS matrix, constant parameters derived from literature [45,46] were used for the 3D printing process. Two different printing raster angle were used to determine the effect of patterning on the tensile properties. The raster angle specifies the direction of the raster pattern relative to the X axis of the print bed, as shown in Fig. 2.

2.4. Tensile testing

Mechanical properties of MWCNTs filled ABS composite tensile specimens prepared based on ASTM D412 A standard were studied using Instron universal testing machine (model 5965). The as scaled dimensions of the dog bone tensile samples were 45 × 9 x 2 mm3 length x width x thickness. The gauge length of the samples was fixed at 40 mm. The cross head speed was kept at 2 mm/min for tensile testing. The elongation values obtained from a transverse device are read through an encoder connected to the front part of the traverse moving motor.

3. Results and discussions

Fig. 1 shows the overall method for nano-composite filament preparation and 3D printing. As mentioned before homogenous distribution of the nano-particles in the ABS matrix is extremely important for successful results. Therefore, a double-screw extruder with a mixing chamber volume of 15 cc was initially used to achieve necessary homogenous dispersions of MWCNTs and ABS. The calculated weight of each constituents of the filament samples fed into the extruder chamber to achieve the wt.% 1 - 10 MWCNTs loading is given in Table 2. After ensuring a homogenous dispersion, a standard filament that can be used

Table 2
The material contents of the sample filament.

No	MWCNT (g)	ABS (g)	Ratio (wt.%)
1	0.15	14.85	1
2	0.45	14.55	3
3	0.75	14.25	5
4	1.05	13.95	7
5	1.50	13.50	10

in a commercial 3D printing machine was prepared using a single screw extruder. It should be noted here that it is extremely difficult to ensure constant filament diameter as variable diameter was measured (± 150 μm) even after several trials before reaching the optimum parameters given in Section 2.2 for the extrusion of the nano-composite filaments. In order to further reduce the dimensional accuracy a winder system integrated into the single screw extruder system may be tested. The nano-composite filaments were the used in a commercial FDM 3D printer. The most prevalent difficulty experienced during the printing process is nozzle clogging which may be alleviated via achieving a better filament dimensional tolerance. Nevertheless, this problem may also be linked to regional agglomerations of the MWCNT fillers which also jeopardise the ultimate aim of the work in achieving electrically conductive and improved mechanical performance of 3D printed plastics. Another major problem of the nano-composite printed was increasingly brittleness of the filament with higher percentage of MWCNTs loading as it causes filament to break abruptly during the process.

Despite all of these mentioned difficulties to be addressed in future work on process optimisation, dog-bone samples with the MWCNTs filled nano-composites has been successfully produced after long try and error tests to evaluate both the mechanical as well as the electrical properties. Test results has been carefully analysed and reported below.

3.1. Tensile properties of 3D printed MWCNTs/ABS composite

Tensile strength, Young's modulus and elongation of the MWCNTs/ABS nano-composite samples are shown in Fig. 3. Change in these properties with respect to weight percentage of MWCNTs in the ABS blank as well as the raster angle are significant. Clearly from the figure, for raster angle [0, 90] the ultimate tensile strength (UTS) is first slightly decreased to 40 MPa for %1 MWCNTs loading after which the UTS is enhanced with increase in MWCNTs loading up to 58 MPa for %7 MWCNTs loading, Fig. 3(a).

The initial decrease in UTS is most likely due to improper interfacial adhesion with the ABS matrix. This detrimental effect is obviously overcome at a certain wt.% CNT loading threshold (3% in this case). The continuously improved UTS by increased MWCNTs loading up to 7 wt.% from this point onwards can be explained by the high specific mechanical properties and the high aspect ratio combined with the high SSA of the MWCNTs. However, the exploitation of the provided interface is also playing a major role concerning the improvement of mechanical properties. The dispersion of the CNTs and the interfacial adhesion to the ABS matrix are therefore key issues in the development of nano-composites. A chemical functionalisation of the CNT surface is also an important approach to improve both interfacial bonding and dispersibility. Unlike some literatures showing reduced strength at

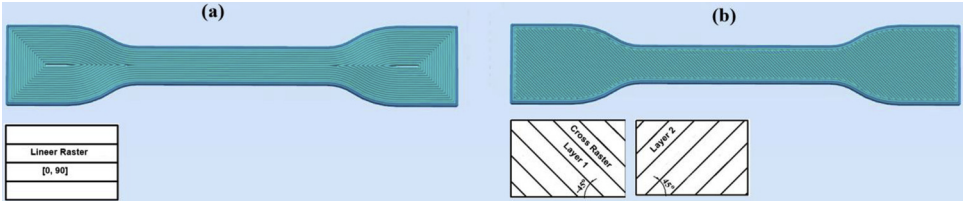

Fig. 2. Illustration of raster angle and printing prewiew.

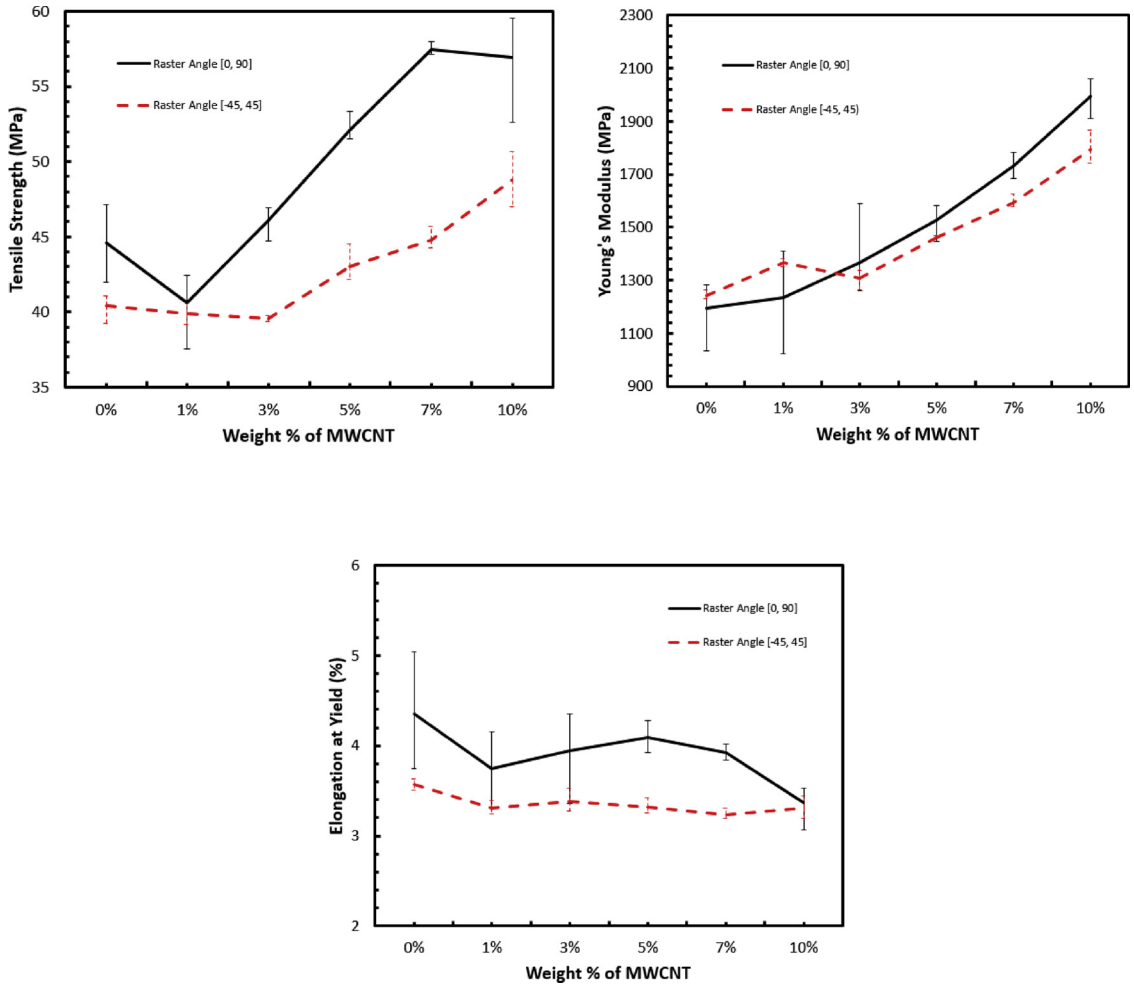

Fig. 3. Change in (a) Tensile strength (b) Elastic modulus (c) Tensile elongation at yield of 3D printed MWCNTs/ABS composite test specimens with respect to weight % of CNTs in the blank ABS.

higher MWCNTs loading [4] involving extrusion free form fabrication, we report here the strength of the MWCNTs loaded ABS nano-composite can be increased up to 7% when FDM 3d printed. This proves that additional 3D printing process enhances fibre alignment and dispersion which are key issues in the development of nano-composites as mentioned above.

But for reinforcements above 7 wt.%, the composite reached the maximum UTS level. At higher filler contents UTS began to decrease which can be attributed to a likely increasing amount of improper impregnated agglomerates, acting as imperfections in the composite (Fig. 9(f)). The overall UTS increase is 288% for %7 MWCNTs loading as compared to blank ABS. In raster angle [-45, 45], %1 and %3 MWCNTs loaded sample shows almost the same UTS as blank ABS, however slightly lower than the [0, 90] layers. At subsequent reinforcement ratios it increased to 4875 MPa for 10% MWCNT loading. The overall UTS increase is 206% for %10 MWCNTs loading as compared to blank (Fig. 4). This is below what is achieved for [0, 90] layering by approximately 10%. The higher UTS in linear layering [0, 90] is believed to be due to uniaxial loading along the CNTs during the tensile test which is not the case in crossed [-45, 45] layering.

The dissimilarity of Young's modulus with various wt.% of MWCNTs loading is emphasized in Fig. 3(b). The change in Young's modulus of raster angle [0, 90] is not discernable for samples loaded with 1% MWCNTs (only 1% increase is measured). Young's modulus significantly increased for all other loading percentages, Fig. 3(b) There is almost a linear increase for 3, 5, 7, 10% MWCNTs loading with maximum achieved at 10% (668% increase over blank ABS). In raster angle [-45, 45], the increase in the Young modulus followed the almost same trend as the linear raster, however with some lower modulus values measured. The fact that elastic modulus is higher with MWCNT loaded samples shows the nano-composite material tend to increasingly resemble the filler MWCNT mechanical stiffness properties with increasing loading rates.

The percentage elongation at yield in blank ABS and MWCNTs/ABS nano-composites are shown in Fig. 3(c). Percentage yield elongation decreases when compared to ABS. This means there is clear transition from ductile to brittle behavior with MWCNTs loading, especially at higher rates. In raster angle [0, 90], this breaking point can be identified between the blank ABS and %1 MWCNTs loading where a sudden decline in the elongation occurred. The region between blank ABS and %1 MWCNTs loading is therefore considered as a ductile to brittle transition zone. From %1 MWCNTs loading and onwards, the entire 3D printed ABS polymer nano-composite samples indicate a brittle behavior. This phenomenon can be observed in the fractured test specimens for both MWCNTs loaded and blank ABS given in Fig. 5. Overall the elongation is decreased by 30% for maximum %10 MWCNTs loading as compared to blank ABS. This can be seen in stress-strain diagram for a key result sample is also shown in Fig.4.

Although significant mechanical strength can be achieved for the MWCNTs filled samples with respect to blank ABS functionalization specific to the MWNT/polymer combination will be necessary in increasing the matrix/filler bonding and hence achieving further mechanical strength performance. It should also be noted a high degree of alignment of MWCNTs with the loading direction was found to be

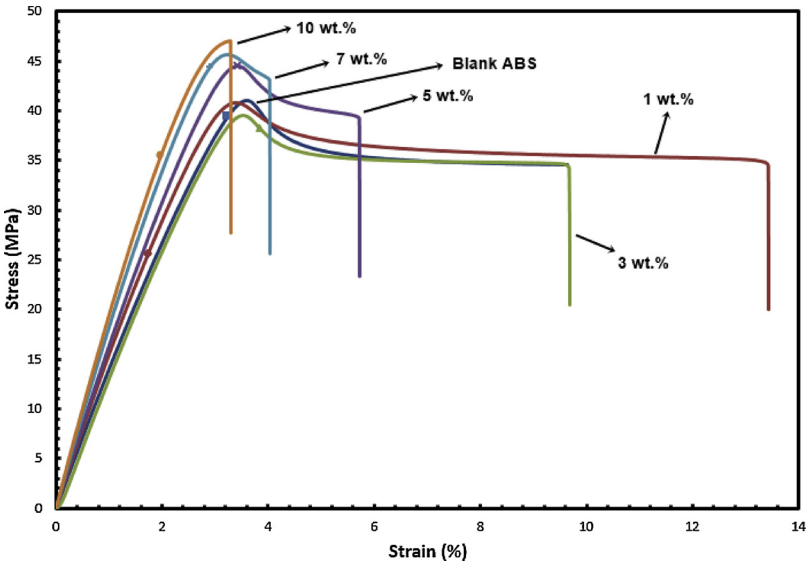

Fig. 4. Stress/Strain diagram of MWCNT/ABS tensile test specimen.

important as the raster angle [-45, 45] results in discernably lower mechanical properties.

3.2. Raman spectroscopy

Raman Spectroscopy were performed to understand the affiliation status between the ABS polymer and MWCNTs in the nano-composite samples. The measurements were carried out using a Raman spectrometer (WiTec, Germany) equipped with a piezo scanner. The excitation laser source was 785 nm wavelength solid state laser. The spectrometer incorporated a cooled charge-coupled device (CCD) detector that operated at −60 °C. All measurements were performed at room temperature. A microscope lens with x20 objective was used. A motorized positioner focused the laser beam on the sample. Raman spectra are recorded from 200 to 1700 cm^{-1}. A typical spectrum was taken with 10 s integration and ten accumulation times, for a total exposure time of 100 s. The laser power at the sample was 5 mW with the 785 nm laser, measured using a Thorlabs power meter and accurate to ~5%.

Spectra obtained from a Standard Raman measurement of ABS and MWCNTs/ABS composites are shown in Fig. 6. The intensity changes of the scattered light from a blank ABS sample (presented in Fig. 6(a)) as a function of calculated wavenumber include many characteristic peaks. One such characteristic peak from the Raman spectrum of blank ABS is at 1352 cm^{-1} (Fig. 6(a)). Clearly from the figure this peak is shifted to 1329 cm^{-1}, 1322 cm^{-1}, 1324 cm^{-1} and 1297 cm^{-1} for 1, 3, 5 and 7% MWCNT loading respectively. This shift can only be explained with the MWCNTs loading ratio and their affinity with the ABS molecules. In line with the tensile strength enhancement observed in Fig. 6(a) these peaks were shifted more significantly for higher MWCNTs loaded samples.

3.3. Electrical properties

The electrical conductivity of the specimens was measured by Keithley 2400 SourceMeter electrical tester apparatus. The measurements were performed on 4 different points of tensile test specimens with different point to point spacing. Fig. 7. shows the electrical conductivity of blank ABS and MWCNTs/ABS nano-composite samples in S/cm. The blank ABS samples shows nonconducting dielectric behavior. From dielectric insulator to conductor conversion is achieved when only 3% addition of MWCNTs for the raster angle [0, 90]. This trend of enhancing electrical conductivity is more pronounced and continue with further addition of the nano-particle (MWCNTs) up to 5 wt.% loading. However, a less discernable effect of further increasing MWCNTs addition on electrical conductivity is also evident from the figure. The sample with a raster angle [0, 90] has begun to show a conductive property at a lower reinforcement ratio than the raster angle

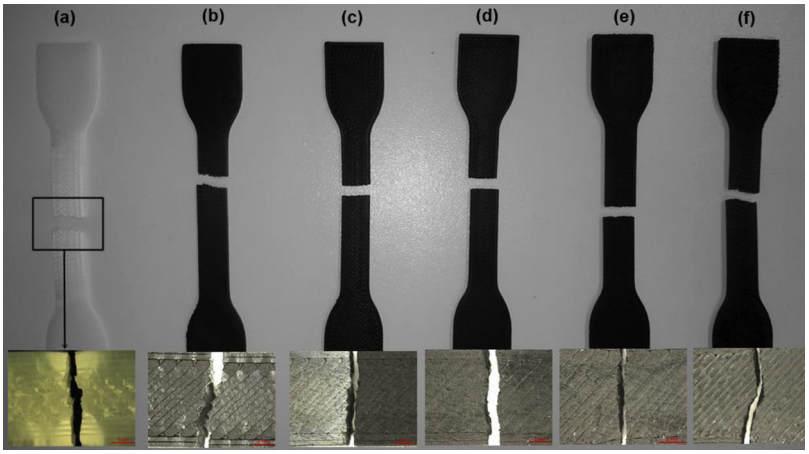

Fig. 5. MWCNTs/ABS tensile test specimens after fracture (a) blank ABS, (b) 1% wt MWCNT, (c) 3% wt MWCNT, (d) 5% wt MWCNT, (e) 7% wt MWCNT, (f) 10% wt MWCNT and before g) blank ABS, (h) 1% wt MWCNT testing.

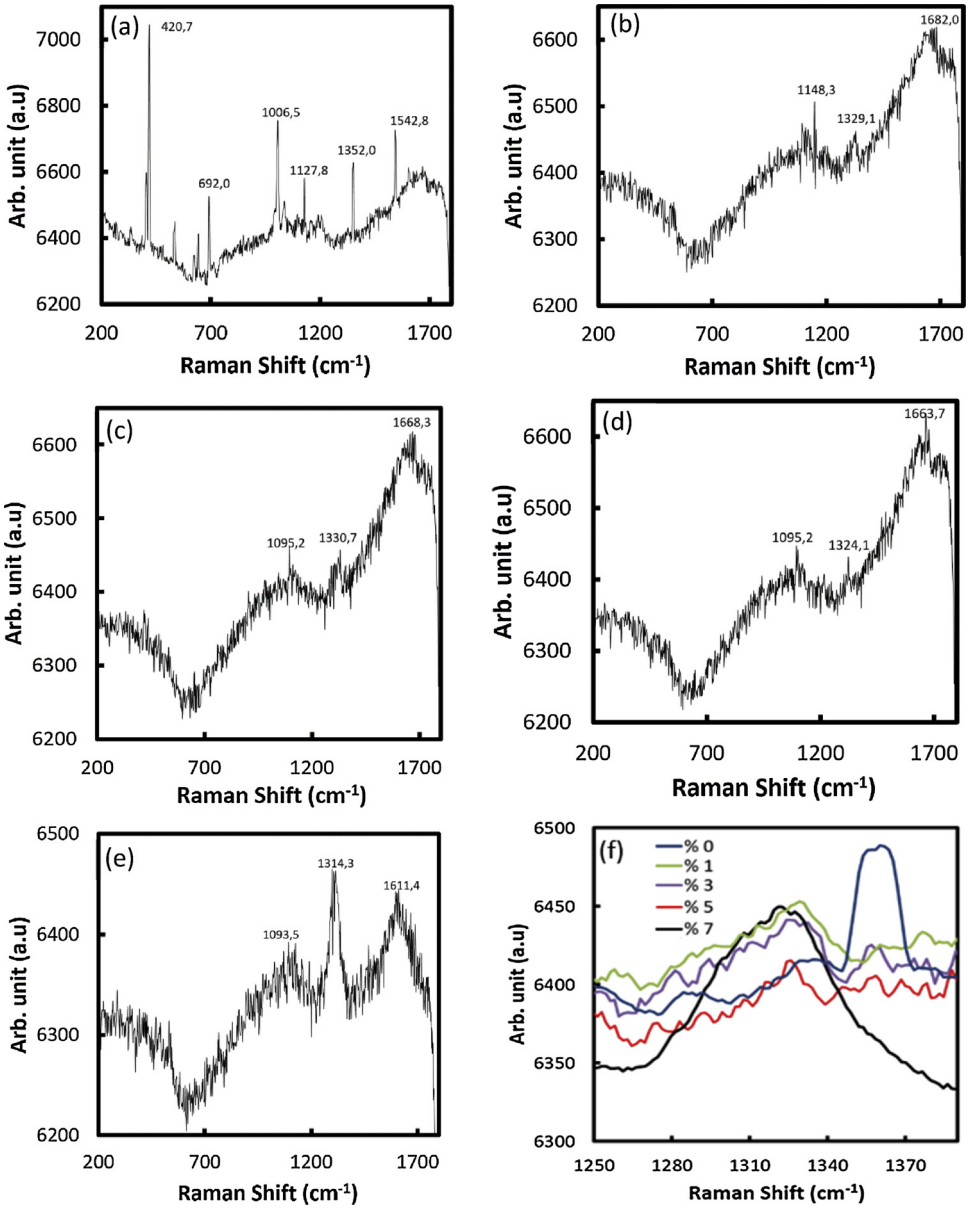

Fig. 6. Raman spectra of 3D printed MWCNTs/ABS test specimens (a) blank ABS (b) with MWCNT loading (wt % of 1) (c) with MWCNT loading (wt % of 3) (d) with MWCNT loading (wt % of 5) (e) with MWCNT loading (wt % of 7) (f) peak shift for various wt% MWCNTs loading.

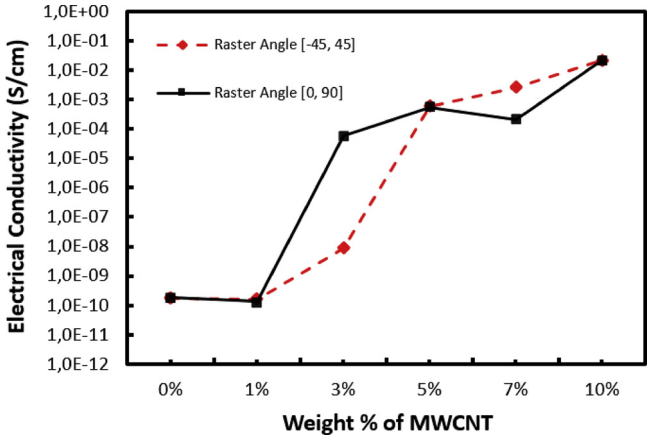

Fig. 7. Electrical conductivity of 3D printed MWCNTs/ABS composite with different weigth percentages of MWCNTs.

[-45, 45]. This is because traces in the raster angle [-45, 45] are discontinuous due to cross layers. As printing continuity is provided in a raster angle [0, 90], electrical conductivity is provided at a lower reinforcement rate.

Therefore, 3D printed MWCNT / ABS nano-composites shows superior properties not only in mechanical strength but also electrical properties with significantly enhanced conductivity. Considerably high electrical properties of MWCNTs filled polymeric composite materials have been demonstrated [38]. The conductivity of the MWCNTs filled ABS show a critical behavior with the fraction of the CNT component reaching the percolation threshold at 3 wt.% loading. At this point the insulator to conductor transition occurs. The behavior of the conductivity of the MWCNTs loaded ABS composite show a smooth transition from resistivity of the dielectric ABS to the conductivity of the CNT component.

In CNT/polymer composites tunneled currents is normally obtained as a function of tunneling distance and matrix material. When a well-dispersed CNT is present at a tunnel opening of less than 1.8 nm in a given matrix free volume, the electrical leakage is theoretically the

Table 3
Process parameters for Melt Flow Index measurements.

Preheating Temp. - °C	235
Nozzle Temp. - °C	235
Load - kg	5
Time - sec	12

lowest. The critical volume fraction of the filler material for forming the percolation network can be less than 1% and greater than 20%, depending on the orientation and the aspect ratio of the fillers. According to Grossiord et al. the formation of the percolation network occurs only at the critical nano-particle loading volume fraction which can be less than 1% to more than 20% depending on the orientation and aspect ratio of the fillers for [38]. Singh et al. also studied phenomenon for different length of MWCNTs in polymer matrix nano-composites [34]. The study showed that, besides volume fraction and orientation, the length of MWCNTs also has significant effect with lower percolation threshold achieved for long MWCNTs based nano-composites. The long MWCNTs with aspect ratio of 157 used in this study enabled to reach the percolation threshold at only 3 wt.% of loading.

3.4. Melt Flow Index (MFI)

The MFI test determines the fluidity of the molten composite by using a constant load to push the melt through a standard orifice [35]. The MFI values of nano-composite specimens were measured by Coesfield Material Test Meltflixer LT with process parameters given in Table 3.

Fig. 8. shows the melt flow index of blank ABS and MWCNTs/ABS composite. MFI is first slightly decreased for %1 MWCNTs. Above this reinforcement value, MFI values are significantly decreased. For the sample containing 10% MWCNT, the MFI value is 164 times less as compared to pure ABS. It should be noted that dispersion with low MFI value makes composite filament extrusion difficult and causes filament breakage. For this reason, composite specimens containing more MWCNTs loadings could not be produced.

3.5. Scanning electron microscopy (SEM)

The fracture surfaces of composites give first information about fracture mechanisms and the influence of particle modification on the fracture behavior. Therefore the 3D-printed MWCNTs/ABS nano-composite samples has also been analysed using a JEOL JSM-6060 LW model Scanning Electron Microscopy machine. The SEM imaged fracture surfaces were taken from similar areas of the failed specimens.

As mentioned before the homogenous dispersion and distribution of

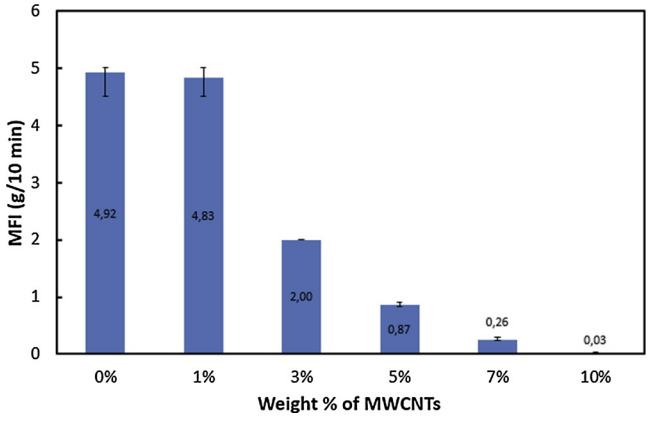

Fig. 8. MFI of 3D printed MWCNTs/ABS composite with different weigth percentages of MWCNTs.

the reinforcing nano-particles (i.e. MWCNTs) in ABS matrix is a vital benchmark for the substantial property enhancement of the 3D printed nano-composites. The morphological features as well as the MWCNTs distribution can be seen in SEM micrographs given in Fig. 9 (a–f). Clearly from the figure, the fracture surface of the MWCNTs loaded samples are significantly different from the blank ABS. Spiky surface in the latter reflects more ductile fracture behavior as compared to MWCNTs loaded samples. All other samples show existence and homogenous distribution of MWCNT (can be diffrenciated from ABS matrix by contrast) except the 1 wt.% loading in which case regional MWCNT agglomarations was detected through EDS analysis attached to SEM. The general toughening effect of nano-particles reflects itself in a considerably larger roughness of the fracture surface of the sample containing 3–10 wt.% CNTs loading. This effect is therefore believed to be related to the general existence of particle reinforcements. Furthermore, the images clearly show that the combined twin screw micro compounder mixing and single screw filament extrusion followed by 3D printing processes uniformly dispersed the MWCNTs throughout the matrix with no porosity as shown Fig. 9(c–f). The agglomarations mentioned for the 1 wt.% case could be the reason for decreased UTS. For the 10 wt.% loading case, although individual MWCNTs chains are separated with no clear agglomarations, regional MWCNT dense regions, we call bunching, were detected as shown in Fig. 10. This phenomenon is most likely related to the observed decrease in both UTS and elongation after 7 wt.% MWCNT loading.

4. Conclusisons

MWCNTs/ABS nano-composite filaments suitable for FDM 3D printing were prepared utilising a micro twin-screw having a back flow channel as well as single screw extruder. As confirmed by SEM imaging, MWCNTs were dispersed and distributed in the ABS polymer matrix uniformly. Tensile test results clearly suggest that specimens with higher MWCNT ratio are stronger than specimens with lower and that raster orientation has a significant effect on the mechanical properties of material. This conclusion was also confirmed by Raman Spectroscopy. In line with the tensile strength enhancement observed, peaks were shifted more significantly for higher MWCNTs loaded samples. On the other hand lower percentage (i.e. 1 wt. %) MWCNTs loaded samples caused nano-particle agglomarations whilst higher percentage loading (i.e. 10 wt.%) caused nano-particle bunching. In both cases mechanical strength of the nano-composite tend to decrease. Raster angle [0, 90] is showed much better mechanical properties than raster angle [-45, 45]. For raster angle [0, 90], the ultimate tensile strength (UTS) is first slightly decreased for %1 MWCNTs. Beyond this loading the UTS is enhanced; 288% of increase for %7 MWCNTs loading is obtained as compared to blank ABS samples. Dielectric behaviors of the nano-composites were investigated to determine current conduction mechanisms and the development of the conductive network within the polymer matrix as a function of MWCNT concentration. There is a good agreement between the values obtained using the data in this work and elsewhere. The lowest value of percolation threshold observed here is endorsed to prolonged twin screw extruder mixing of the agglomerate of high aspect ratio MWCNTs in the ABS matrix, subjected to even dispersal. The conductivity of the MWCNTs filled ABS showed a critical behavior with the fraction of the CNT component reaching the percolation threshold at 3 wt.% loading for raster angle [0, 90]. The highest electrical conductivity value achieved for the %10 MWCNTs loading was 232 e^{-2} S/cm. MFI values dramatically decreases with MWCNTs loading, reaching 0.03 g/10 mm value for %10 loading, explaining nozzle clogging problem during the 3D printing process using filaments with higher MWCNT filler rates

Acknowledgements

This work was supported by TÜBİTAK BİDEB [grant numbers

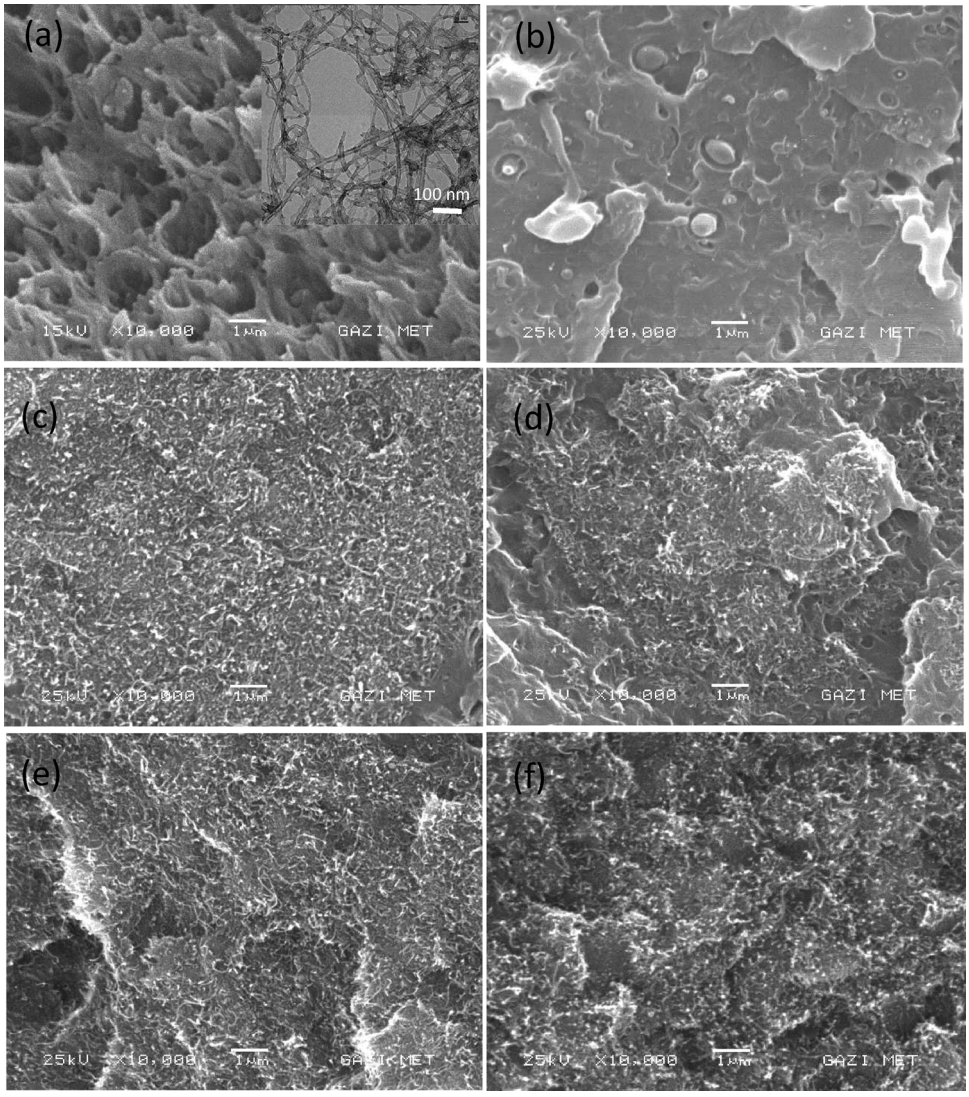

Fig. 9. SEM images of the 3D printed MWCNTs/ABS tensile test specimen fracture surfaces (a) blank ABS and raw MWCNT at right corner, (b) 1% wt, (c) 3% wt, (d) 5% wt, (e) 7% wt, (f) 10% wt MWCNT loading percentages (MWCNTs can be diffrenciated by contrast).

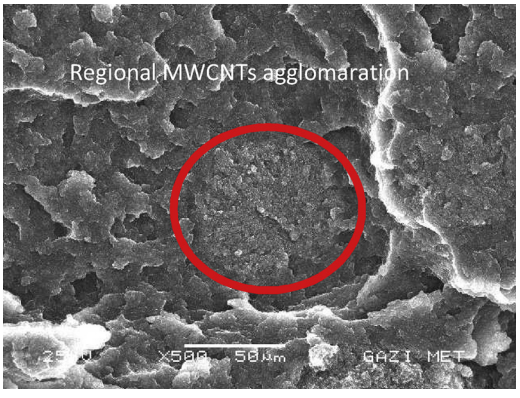

Fig. 10. SEM image of the 3D printed MWCNTs/ABS tensile test specimen fracture surface - 10% wt MWCNT loading showing MWCNT agglomaration.

115096, 2015].

References

[1] Standard terminology for additive manufacturing technologies. West Conshohocken: ASTM International; 2010.
[2] Chua CK, Leong KF, Lim CS. Rapid prototyping: principles and applications. 3rd ed. World Scientific; 2010.
[3] Upcraft S, Fletcher R. The rapid prototyping technologies. Assembly Autom 2003;23(4):318–30.
[4] Kruth JP, Wang X, Laoui T, Froyen L. Lasers and materials in selective laser sintering. Assembly Autom 2003;23(4):357–71.
[5] Li X, Wang CT, Zhang WG, Li YC. Fabrication and characterization of porous Ti6Al4V parts for biomedical applications using electron beam melting process. Mater Lett 2009;63(3):403–5.
[6] Cooke MN, Fisher JP, Dean D, Rimnac C, Mikos AG. Use of stereolithography to manufacture critical sized 3D biodegradable scaffolds for bone ingrowth. J Biomed Mater Res Part B Appl Biomater 2002;64(B):65–9.
[7] Dudek P. FDM 3D printing technology in manufacturing composite elements. Arch Metall Mater 2013;58(4):1415–8.
[8] Comb JW, Priedeman WR, Leavit PJ, Skubic RL, Batchelder JS. High-precision modeling filament. United States patent US6866807B2. 2005 Sept 21.
[9] Ford S, Despeisse M. Additive manufacturing and sustainability: an exploratory study of the advantages and challenges. J Clean Prod 2016;137:1573–87.
[10] Kennedy ZC, Christ JF, Evans KA, Arey BW, Sweet LE, Warner MG, Erikson RL, Barrett CA. 3D-printed poly(vinylidene fluoride)/carbon nanotube composites as a tunable, low-cost chemical vapour sensing platform. Nanoscale 2017;9:5458–66.
[11] Marcincinova LN, Marcincin JN, Barna J, Torok J. Special materials used in FDM rapid prototyping technology application. Proceedings of IEEE 16th International Conference on Intelligent Engineering Systems 2012:73–6.
[12] Ivanova OW, Christopher BC, Thomas I, Olga W, Christopher CT. Additive manufacturing (AM) and nanotechnology: promises and challenges. Rapid Prototyping J 2013;19(5):353–64.
[13] Shofner ML, Rodríguez-Macías FJ, Vaidyanathan R, Barrera EV. Single wall nanotube and vapor grown carbon fiber reinforced polymers processed by extrusion freeform fabrication. Compos Part A-Appl S 2003;34(12):1207–17.

[14] George T, Eirini T, Constantinos S. Comparative study on nanotubes reinforced with carbon filaments for the 3D printing of mechanical parts. World Trans Eng Technol Educ 2014;12(3):392–6.
[15] Tekinalp HL, Kunc V, Velez-Garcia GM, Duty CE, Love LJ, Naskar AK. Highly oriented carbon fiber-polymer composites via additive manufacturing. Compos Sci Technol 2014;105(10):144–50.
[16] Shofner ML, Lozano K, Rodríguez-Macías FJ, Barrera EV. Nanofiber reinforced polymers prepared by fused deposition modeling. J Appl Polym Sci 2003;89(11):3081–90.
[17] Leigh SJ, Bradley RJ, Purssell CP, Billson D, Hutchins DA. A simple, low-cost conductive composite material for 3D printing of electronic sensors. PLoS One 2012;7(11):1–7.
[18] Postiglione G, Natale G, Griffini G, Levi M, Turri S. Conductive 3D microstructures by direct 3D printing of polymer/carbon nanotube nanocomposites via liquid deposition modeling. Compos Part A Appl Sci Manuf 2015;76(2015):110–4.
[19] Gnanasekarana K, Heijmansa T, van Bennekomb S, Woldhuisb H, Wijniab S, et al. 3D printing of CNT- and graphene-based conductive polymer nanocomposites by fused deposition modeling. Appl Mater Today 2017;9:21–8.
[20] Aliheidari N, Hohimer C, Ameli A. 3D-Printed conductive nanocomposites for liquid sensing applications. ASME; 2017.
[21] Scheirs J. A guide to polymeric geomembranes: a practical approach. John Wiley & Sons; 2009. p. 284–6.
[22] Morales TO, Sanchez VS, Ramos LF. Effect of carbon nanofiber functionalization on the dispersion and physical and mechanical properties of polystyrene nanocomposites. Macromol Mater Eng 2006;291(12):1547–55.
[23] Sahooa NG, Ranab S, Chob JW, Lia L, Chana SH. Polymer nanocomposites based on functionalized carbon nanotubes. Prog Polym Sci 2010;35(7):837–67.
[24] Moniruzzaman M, Winey KI. Polymer nanocomposites containing carbon nanotubes. Macromolecules 2006;39(16):5194–205.
[25] Kim JY, Han SI, Kim SH. Crystallization behaviors and mechanical properties of poly(ethylene 2,6-naphthalate)/multiwall carbon nanotube nanocomposites. Polym Eng Sci 2007;47(11):1715–23.
[26] Jin SH, Park YB, Yoon KH. Rheological and mechanical properties of surface modified multi-walled carbon nanotube-filled PET composite. Compos Sci Technol 2007;67(15):3434–41.
[27] Wang Z, Ciselli P, Peijs T. The extraordinary reinforcing efficiency of single-walled carbon nanotubes in oriented poly(vinyl alcohol) tapes. Nanotechnology 2007;18(45). 455709/1–9.
[28] Yang BX, Shi JH, Pramoda KP, Goh SH. Enhancement of stiffness, strength, ductility and toughness of poly(ethylene oxide) using phenoxy-grafted multiwalled carbon nanotubes. Nanotechnology 2007;18(12). 125606/1–7.
[29] Ajayan PM, Stephan O, Colliex C, Trauth D. Aligned carbon nanotube arrays formed by cutting a polymer resin-nanotube composite. Science 1994;265(5176):1212–4.
[30] Jamal A, Ali R, Somayeh M. Preparation and characterization of linear low density polyethylene/carbon nanotube nanocomposites. J Macromol Sci Part B: Phys 2007;46(5):877–89.
[31] Li L, Li CY, Ni C, Rong LX, Hsiao B. Structure and crystallization behavior of Nylon 66/multi-walled carbon nanotube nanocomposites at low carbon nanotube contents. Polymer 2007;48(12):3452–60.
[32] Lee JL, Zhu W, Nowicki M, Lee G, Heo DN, Kim J, Zuo YY, Zhang LG. 3D printing nano conductive multi-walled carbon nanotube scaffolds for nerve regeneration. J Neural Eng 2018;15:016018.
[33] Yu WW, Zhang J, Wu JR, Wang XZ, Deng YH. Incorporation of graphitic nano-filler and poly(lactic acid) in fused deposition modeling. J Appl Polym Sci 2017;134. 44703.
[34] Kwok SW, Goh KHK, Tan ZD, Tan STM, Tjiu WW, Soh JY, et al. Electrically conductive filament for 3D-printed circuits and sensors. Appl Mater Today 2017;9:167–75.
[35] Kumar N, Jain PK, Tandon P, Pandey PM. Additive manufacturing of flexible electrically conductive polymer composites via CNC-assisted fused layer modeling process. J Braz Soc Mech Sci Eng 2018;40:175.
[36] Christ JF, Aliheidari N, Ameli A, Pötschke P. 3D printed highly elastic strain sensors of multiwalled carbon nanotube/thermoplastic polyurethane nanocomposites. Mater Des 2017;131:394–401.
[37] Wei X, Li D, Jiang W, Gu Z, Wang X, Zhang Z, et al. 3D printable graphene composite. Sci Rep 2015;5(11181).
[38] Mu Q, Wang L, Dunn CK, Kuang X, Duan F, Zhang Z, et al. Digital light processing 3D printing of conductive complex structures. Addit Manuf 2017;18:74–83.
[39] Gryshchuk O, Karger KJ, Thomann R, Konya Z, Kiricsi I. Multiwall carbon nanotube modified vinylester and vinylester based hybrid resins. Compos Part A Appl Sci Manuf 2006;37(9):1252–9.
[40] Ghose S, Watson KA, Delozier DM, Working DC, Siochi EJ, Connell JW. Incorporation of multi-walled carbon nanotubes into high temperature resin using dry mixing techniques. Compos Part A Appl Sci Manuf 2006;37(3):465–75.
[41] Bliznyuk VN, Singamaneni S, Sanford RL, Chiappetta D, Crooker B, Shibaev PV. Matrix mediated alignment of single wall carbon nanotubes in polymer composite films. Polymer 2006;47(11):3915–21.
[42] Singh IV, Tanaka M, Zhang J, Endo M. Evaluation of effective thermal conductivity of CNT-based nano-composites by element free Galerkin method. Int J Numer Meth Heat Fluid Flow 2007;17(6):757–69.
[43] Xu S, Rezvanian O, Peters K, Zikry MA. Tunneling effects and electrical conductivity of CNT polymer composites. MRS Proceedings 2011.
[44] Dorigatoa A, Morettia DulaS, Unterbergerb SH, Pegorettia A. Electrically conductive nanocomposites for fused deposition modelling. Synth Met 2017;226:7–14.
[45] Mohamed OA, Masood SH, Bhowmik JL, Nikzad M, Azadmanjiri J. Effect of process parameters on dynamic mechanical performance of FDM PC/ABS printed parts through design of experiment. JMEPEG 2016;25:2922–35.
[46] Rankouhi B, Javadpour S, Delfanian F, Letcher T. Failure analysis and mechanical characterization of 3D printed ABS with respect to layer thickness and orientation. J Fail Anal Preven 2016;16:467–81.